

InSAR monitoring of Krafla, Bjarnarflag and Theistareykir geothermal areas

2023 update





InSAR monitoring of Krafla, Bjarnarflag and Þeistareykir geothermal areas

2023 update

Höfundar
Vincent Drouin

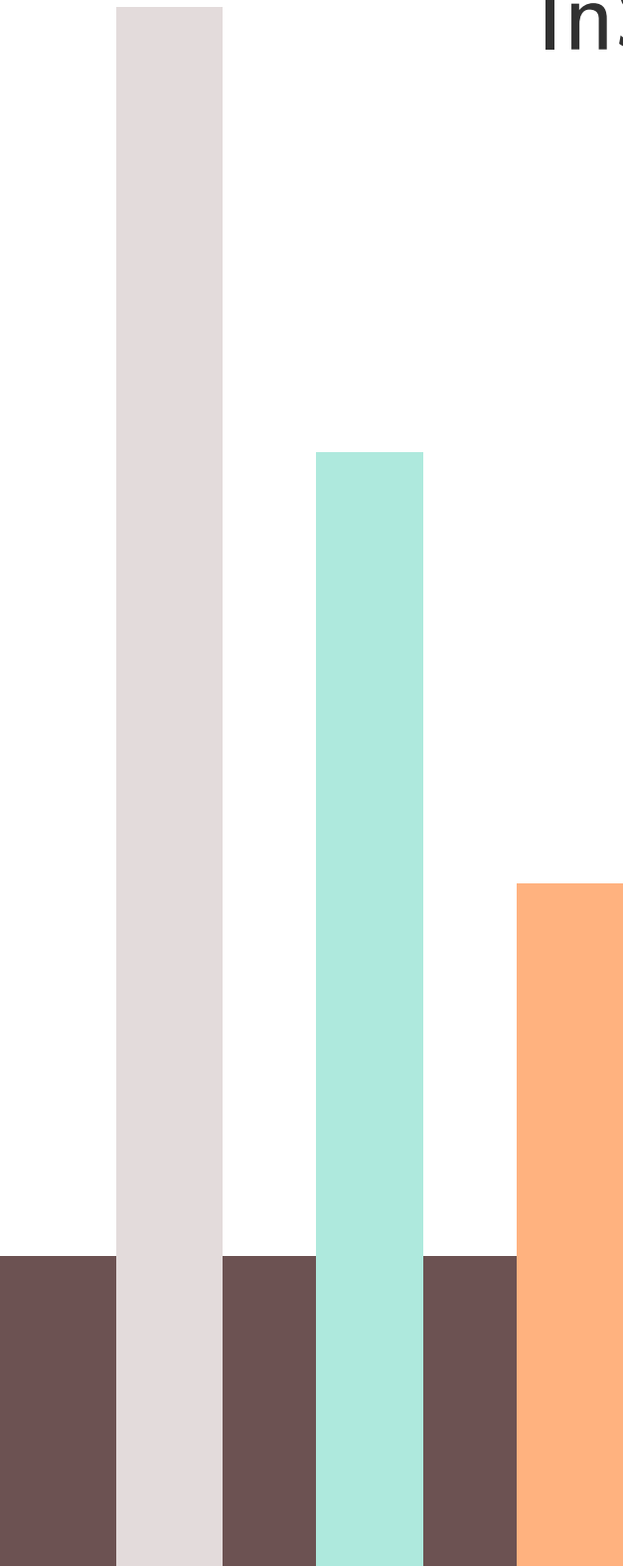
Dagsetning
Desember 2023

Lykilsíða

Skýrsla LV nr	LV-2023-063	Dagsetning	Desember 2023
Fjöldi Síðna	27	Upplag	1
Dreifing	<input type="checkbox"/> Birt á vef LV	<input checked="" type="checkbox"/> Opin	<input type="checkbox"/> Takmörkuð til [Dags.]
Titill	InSAR monitoring of Krafla, Bjarnarflag and Þeistareykir geothermal areas – 2023 update		
Höfundar/fyrirtæki	Vincent Drouin		
Verkefnisstjóri	Anette K. Mortensen		
Unnið fyrir	Landsvirkjun		
Samvinnuaðilar	–		
Útdráttur	<p>Synthetic Aperture Radar Interferometry (InSAR) of Sentinel-1 images was used to estimate the deformation at Krafla, Bjarnarflag, and Þeistareykir between summer 2022 and summer 2023.</p> <p>Results shows only small deformation (<5 mm) within the Krafla caldera. The deformation at Bjarnarflag is still stable, at 5-6 mm/yr of subsidence since 1990. At Þeistareykir, the slow subsidence (<5 mm/yr) observed north of Bæjarfjall since the onset of production in 2017 is still ongoing. Similarly, the faster subsidence (10-15 mm/yr) localized near the re-injection boreholes is also constant. However, a broad inflation pattern is observed in the Þeistareykir central volcano. The uplift is centered near an ancient crater row, 2 km west of the power station. The uplift amounts for about 12-13 mm between summer 2022 and 2023. This inflation can be modeled with a point source located at 4.5-5 km with 1.2-1.5 millions m³ volume increase.</p>		
Lykilorð	InSAR, Krafla, Bjarnarflag, Þeistareykir, geothermal, volcano		

Samþykki verkefnisstjóra
Landsvirkjunar

Anette K. Mortensen



InSAR monitoring of Krafla, Bjarnarflag and Peistareykir geothermal areas.

2023 update

Prepared for **Landsvirkjun**

Vincent Drouin

November 30, 2023

Contents

Glossary	2
1 Introduction	3
2 Data & methodology	3
3 Results	5
3.1 Krafla	5
3.2 Bjarnarflag	9
3.3 Peistareykir geothermal field	9
3.4 Peistareykir central volcano	14
4 Discussion	17
References	19
A Appendix	21
A.1 Krafla & Bjarnarflag	21
A.2 Peistareykir	22

Glossary

ascending orbit	When the satellite moves from south to north direction.
descending orbit	When the satellite moves from north to south direction.
GNSS	[Global Navigation Satellite System] Constellation of satellites providing positioning on a global basis. For instance, GPS.
InSAR	[SAR interferometry] Technique consisting in looking at the phase difference between two SAR acquisitions to get information about the ground motion.
LOS	[Line-of-sight] InSAR provides deformation measurements along the line-of-sight of the SAR satellite. This means these are one-dimensional deformation measurement, away or toward the satellite, unlike for instance GNSS measurements which are three-dimensional (East, North, Up).
near-East	Estimation of the deformation along the East direction, derived from combining multiple LOS deformation.
near-Up	Estimation of the deformation along the Up direction, derived from combining multiple LOS deformation.
SAR	[Synthetic Aperture Radar] Technique consisting in using the motion of the radar instrument to improve resolution.

1 Introduction

Krafla and Peistareykir are two active volcanic systems located in the northern part of the Northern Volcanic Zone in Iceland. There are active geothermal fields within both system. These geothermal fields are currently utilised by Landsvirkjun, the National Power Company of Iceland, to produce electricity and direct heating.

The Krafla power station began production in August 1977 with an initial capacity of 30 MW which was extended to 60 MW in 1999. The Bjarnarflag power station, located 8 km SW of the Krafla power station, has been in service since 1969 and has a capacity of 5 MW since 2019 (3 MW earlier). Both power stations are located along the same fissure swarm. A large rifting event with multiple dike intrusions took place within the Krafla volcanic system from 1975 to 1984 (Einarsson, 1991). A magma reservoir located beneath Leirhnjúkur, in the center of the caldera, inflated and deflated multiple time during this event. Following the end of the Krafla Fires in 1984, the magma chamber continued to inflate until 1989. It then started to deflate at a fast rate that quickly slowed down until no movements were visible in the late 1990's (Sturkell et al., 2008). From then on until 2018, the deformation in the area was dominated by subsidence within the Krafla and Bjarnarflag geothermal fields and by subsidence along the fissure swarm (Drouin, Sigmundsson, et al., 2017). Between summer 2018 and summer 2020 a ~ 11 mm/yr uplift was observed between Leirhnjúkur and the power station (Drouin, 2020).

The Peistareykir power station began production in November 2017 and has a current capacity of 90 MW. InSAR measurements since the early 1990's show that two inflation events appear to have taken place within the Peistareykir volcanic system, the first one around 1995 and second one around 2007 (Metzger and Jónsson, 2014). No significant deformation within the geothermal field north of Bæjarfjall was observed prior to the start of production. Between summer 2017 and summer 2020, a new subsidence of about 5 mm/yr is observed between the power station and Bæjarfjall (Drouin, 2020). The subsidence reaches about 15 mm/yr in the vicinity of the injection wells.

2 Data & methodology

Interferometric Synthetic Aperture Radar (InSAR) is a remote sensing technique that allows measurements of surface deformation over large areas. It has been successfully used to observe surface deformation caused by earthquakes, volcanoes, plate tectonics, landslides, glaciers, geothermal utilization, ground-water extraction, etc.

The InSAR principle is to use the phase information of two SAR acquisitions and calculate their difference to generate an interferogram. This interferogram contains various signals: topography, satellite orbits, ground deformation, atmospheric disturbances, and noise. It is possible to extract the deformation signal with time-series analysis. The deformation in the line-of-sight (LOS) of the satellite (i.e. away or toward the satellite) is obtained. An interferogram decorrelates (i.e. loses signal) in areas where the ground surface changes too much between acquisitions. The most common causes are vegetation changes, snow, new constructions, or extremely large deformations. In North Iceland, snow is a main issue, therefore only summer acquisitions (from early June to end of September) are used for InSAR.

There have been many public and commercial SAR satellite missions since the early 1990's. The Sentinel-1 SAR mission (late 2014 - present) is one of the most recent missions and it has been extremely valuable for the InSAR community by providing free-of-charge consistent acquisitions over most of the world. Over Iceland, it provided images every 12 days between 2015 and 2017, every 6 days between 2017 and 2021. Since late December 2021, one of the two Sentinel-1 satellites failed and acquisitions are back to a 12 days repeat time. Each image covers about 240 km wide swath, divided in three sub-swaths of about 80 km. The resolution of a pixel is about 3 m x 14 m.

The images were pre-processed with the Interferometric synthetic aperture radar Scientific Computing Environment, ISCE, (Rosen et al., 2012) before doing the deformation time-series analysis with a in-house implementation of the small-baseline algorithm, SBAS (Berardino et al., 2002). Acquisitions with loss of signal because of snow or with strong atmospheric noise were removed from the analysis.

Three Sentinel-1 tracks covering the areas of interest were analyzed: two tracks on a descending orbits (T9 and T111) and one track on an ascending orbit (T147). The number of images used in the time-series analysis of each of these tracks can be found in Table 1.

Each track has a different point of view over the area of interest. That means it is possible to combine them to extract the East and Up components of the deformation, called near-East and near-Up, respectively, to show the approximation of the decomposition process (Drouin and Sigmundsson, 2019). The North component of the deformation cannot be retrieved because of the near-polar orbits of the satellite.

Table 1: Number of acquisitions selected per summer for each track.

Track	2015	2016	2017	2018	2019	2020	2021	2022	2023	Total
T9	7	7	18	16	18	17	15	11	10	119
T111	9	8	18	16	16	17	13	9	10	116
T147	8	7	17	17	19	14	12	10	10	114

3 Results

3.1 Krafla

The deformation pattern at Krafla between summer 2022 and summer 2023 is fairly complex (Fig. 1). The maximum of subsidence within the Krafla caldera, about 5-7 mm/yr, is located at the south rim of the caldera near Hvíthólar (Fig. 1b). There is also a 5 mm/yr uplift on the west side of the caldera. This uplift is easier to interpret when compared to the velocities prior to 2018 inflation (Fig. 2a). The deviation/difference between these background velocities and the following years velocities shows a clear uplift in the caldera during 2018-2019 and 2019-2020 (Fig. 2b,c). For 2020-2021 and 2021-2022, a general uplift of about 5-6 mm/yr is still visible, with a peak just west of Leirhnjúkur (Fig. 2d,e). And for 2022-2023, the uplift is faster than during 2020-2022 but slower than during 2018-2020 (Fig. 2f). These four phases can also be observed of the time-series plot (Fig. 4): subsidence during 2015-2018, uplift during 2018-2020, slow subsidence during 2020-2022, and slow uplift during 2022-2023. When comparing the pre-inflation 2015-2018 period to the 2018-2023 period, a clear uplift is visible in the center of the caldera (Fig. 3a-c). As expected, it is associated with an horizontal outward motion (Fig. 3f).

At Hvíthólar the subsidence pattern observed during 2022-2023 is similar to the one observed during 2018-2019 and 2021-2022 but at a slower rate (Fig. 2b,e,f). The time-series of vertical deformation at this location shows significant variations with time (Fig. 5). There is subsidence during 2015-2017, 2018-2019, and 2021-2023. There is little to no vertical deformation during 2017-2018 and 2020-2021. There is uplift during 2019-2020. These temporal variations of the vertical deformation show a strong correlation with the extraction rate at borehole KJ-21, the main production well in this area (Drouin, 2022). When geothermal fluids are extracted, there is subsidence and when no extraction occurs, there is minor uplift or no significant vertical deformation.

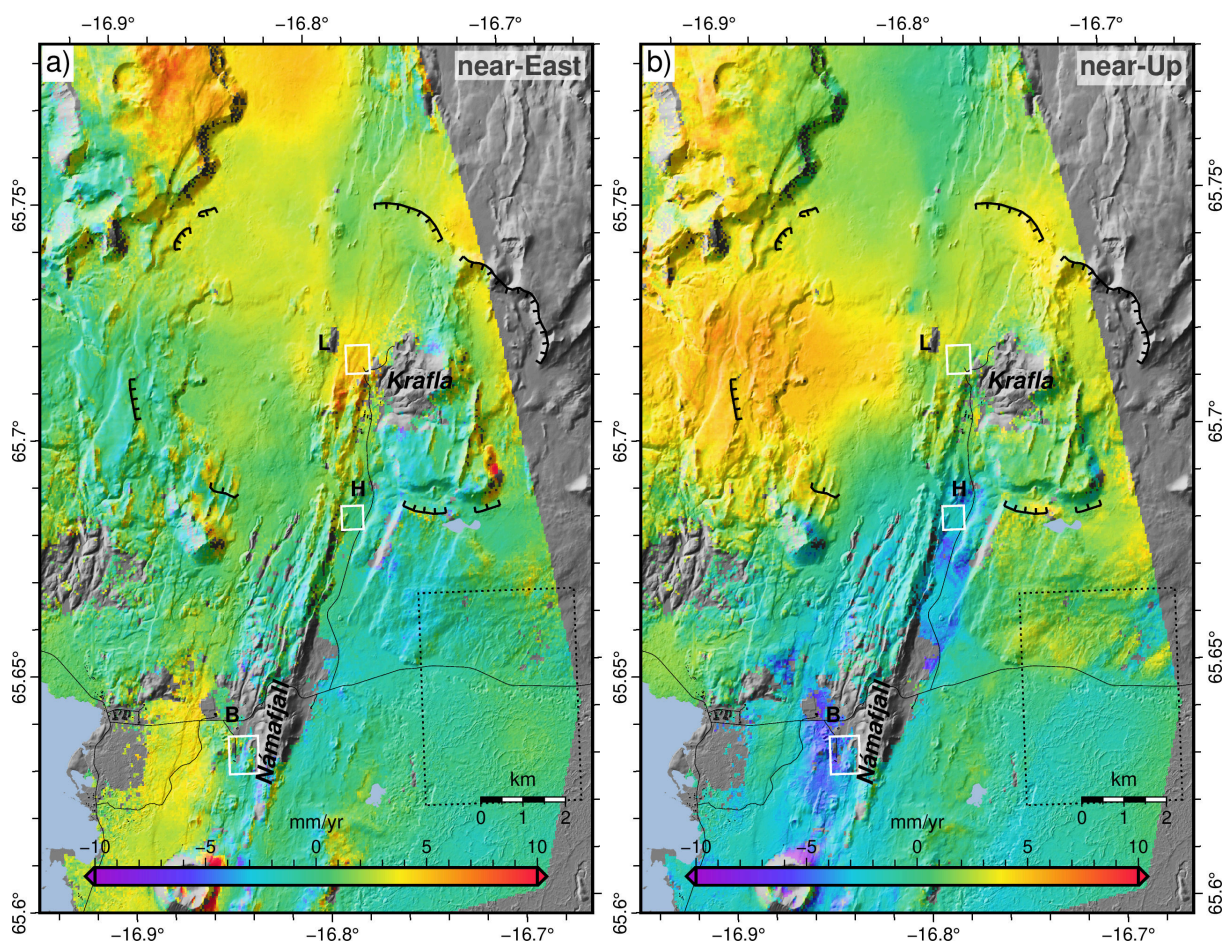


Figure 1: **(a)** Near-East and **(b)** near-Up velocities [mm/yr] between summer 2022 and summer 2023. Leirhnjúkur (L) and Hvíthólar (H) are indicated. White boxes show sampling areas for the time-series plots. Velocities are referenced to the area delimited by the dotted line. Background shows shaded topography, the Krafla caldera boundary (comb line), roads (thin lines), and lakes (blue areas).

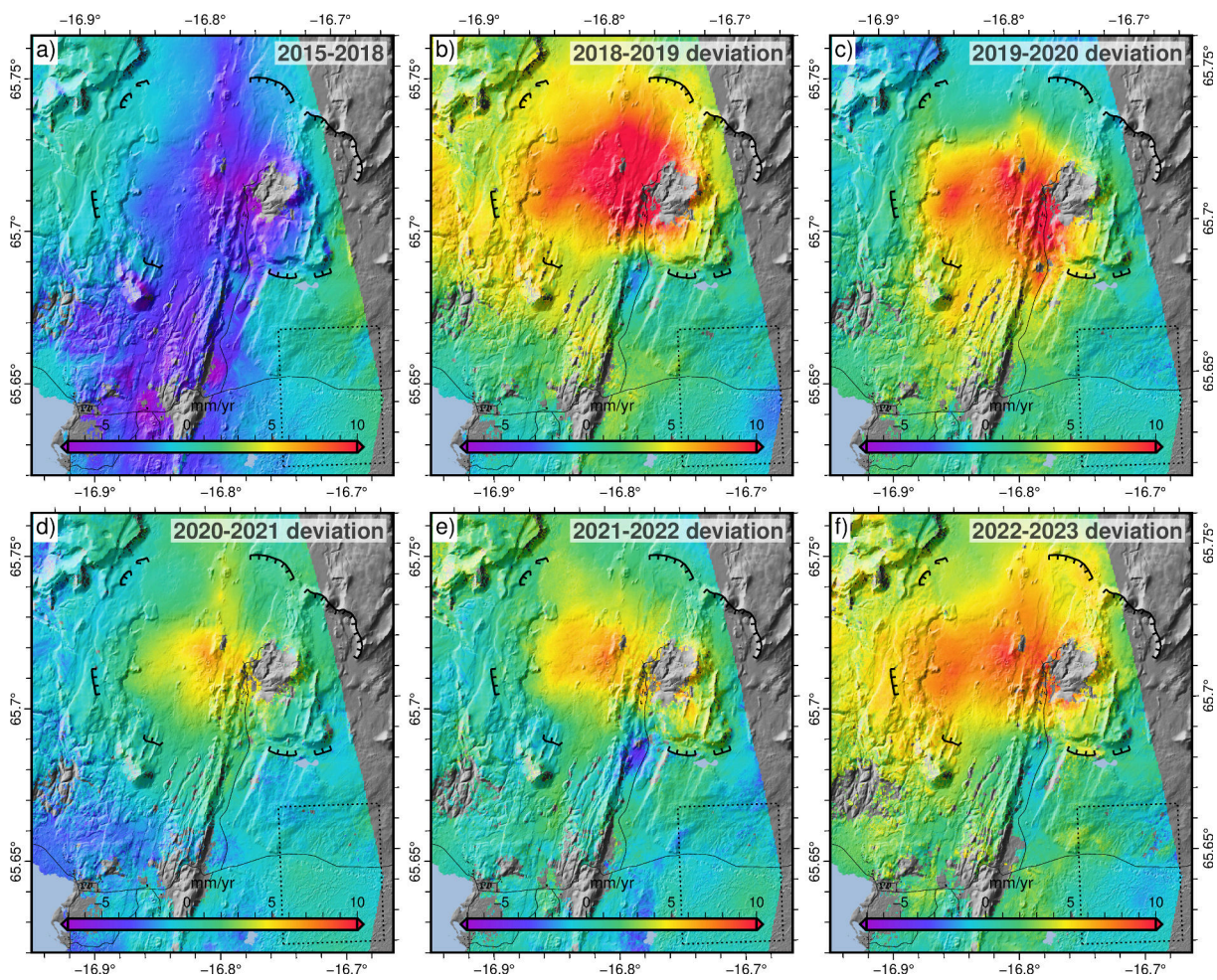


Figure 2: **(a)** Near-Up velocities [mm/yr] for 2015-2018 and **(b-f)** the deviation from it for the following summer-to-summer velocities. Background shows shaded topography, the Krafla caldera boundary (comb line), roads (thin lines), and lakes (blue areas).

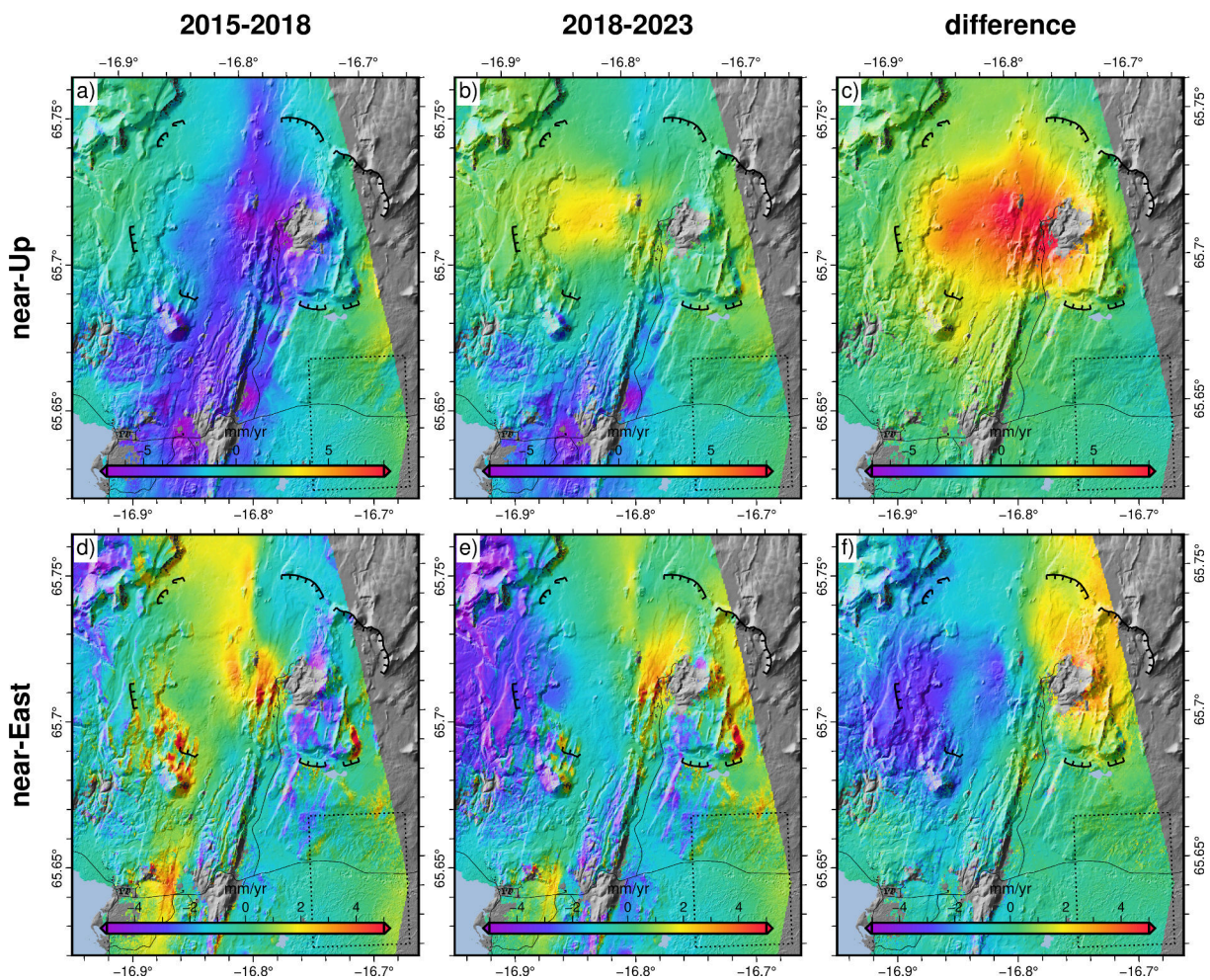


Figure 3: Near-East and near-Up velocities [mm/yr] for 2015-2018, 2018-2023, and the difference between the two periods. Background shows shaded topography, the Krafla caldera boundary (comb line), roads (thin lines), and lakes (blue areas).

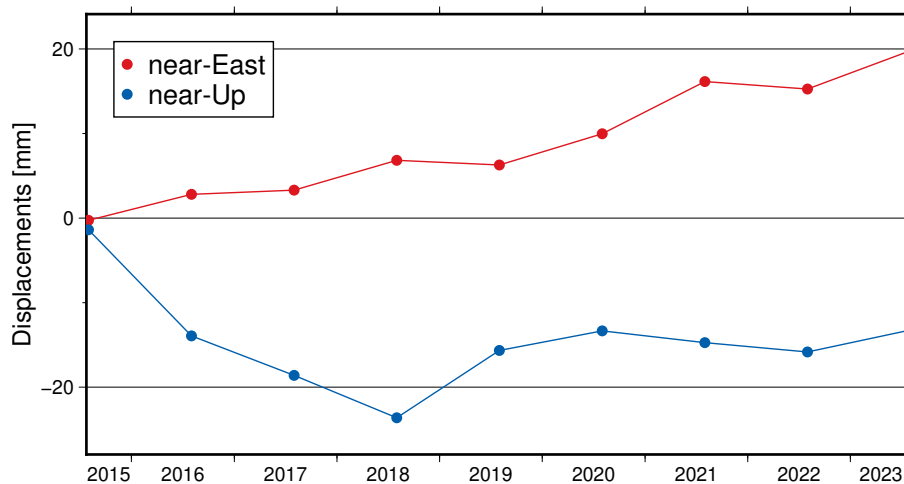


Figure 4: Near-East and Near-Up time-series of deformation near the maximum of uplift during 2018-2020. Location is indicated by the white box between Leirhnjúkur and Krafla on Figure 1.

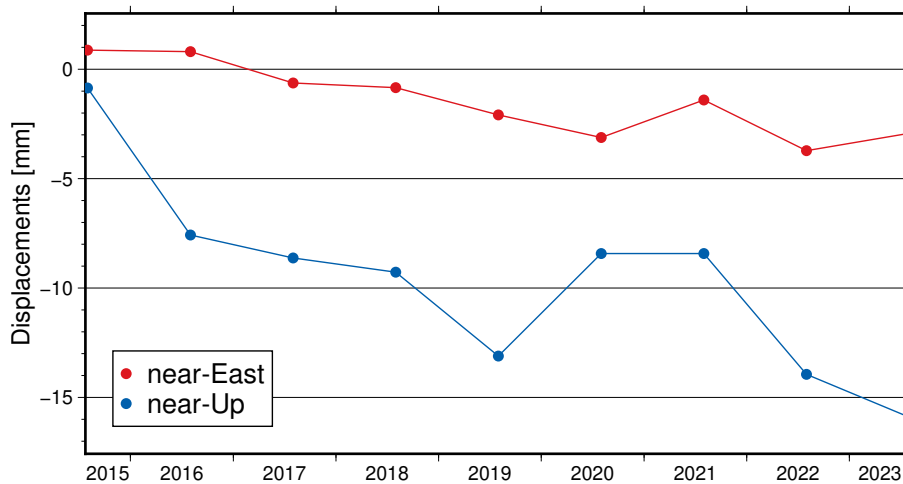


Figure 5: Near-East and Near-Up time-series of deformation near the maximum of uplift during 2018-2020. Location is indicated by the white box next to Hvíthólar on Figure 1.

3.2 Bjarnarflag

Subsidence has been fairly constant at Bjarnarflag since 2015, at rate of about 5-6 mm/yr (Fig. 6). The maximum of subsidence is located west of Bjarnarflag (Fig. 1). There is no change in deformation before and after the inflation at Krafla (Fig. 3).

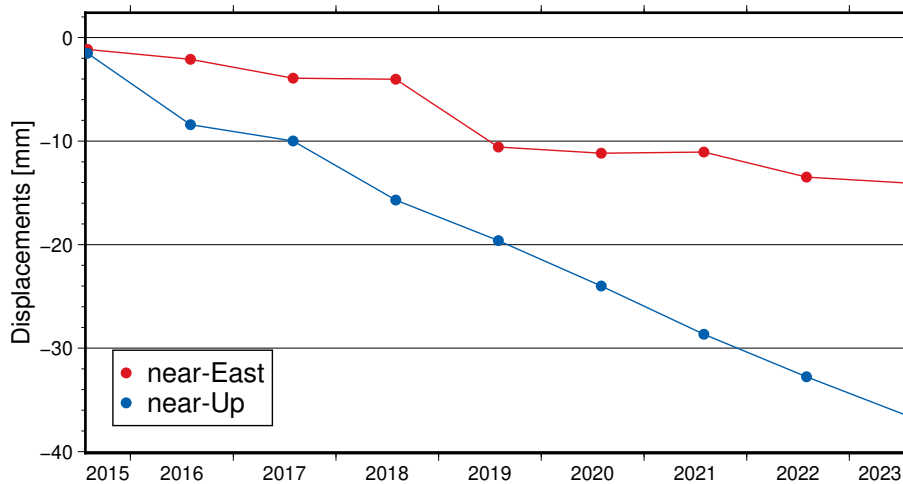


Figure 6: Near-East and Near-Up time-series of deformation at Bjarnarflag. Location is indicated by the white box west of Námarfjall on Figure 1.

3.3 Peistareykir geothermal field

Between summer 2022 and summer 2023, the deformation at Peistareykir is different from the previous years (Fig. 7, see Section 3.4 for more details). However, when focusing on the Peistareykir geothermal field and its immediate surroundings the deformation is similar to what was observed since 2017 (Fig. 8). A 3-4 mm/yr subsidence is visible in the geothermal field, with a local maximum of about 13 mm/yr. The subsidence appears to be bound within

two faults: on the west side by the Tjarnarás fault a few hundred meters west of the road and on the east side by a fault along Ketilfjall. The west side fault is also clearly visible on the near-East velocities (Fig. 9). The subsidence extends approximately from the power station in the north to the middle of Bæjarfjall in the south. The overall subsidence in the geothermal area is >30 mm since 2017 (Fig. 10 and 11). The fastest subsidence is localized in the north-western part of the geothermal field at the location of three injection wells (PN-1, PN-2, PR-12). There, the subsidence is similar to what was measured since 2018 (Fig. 12).

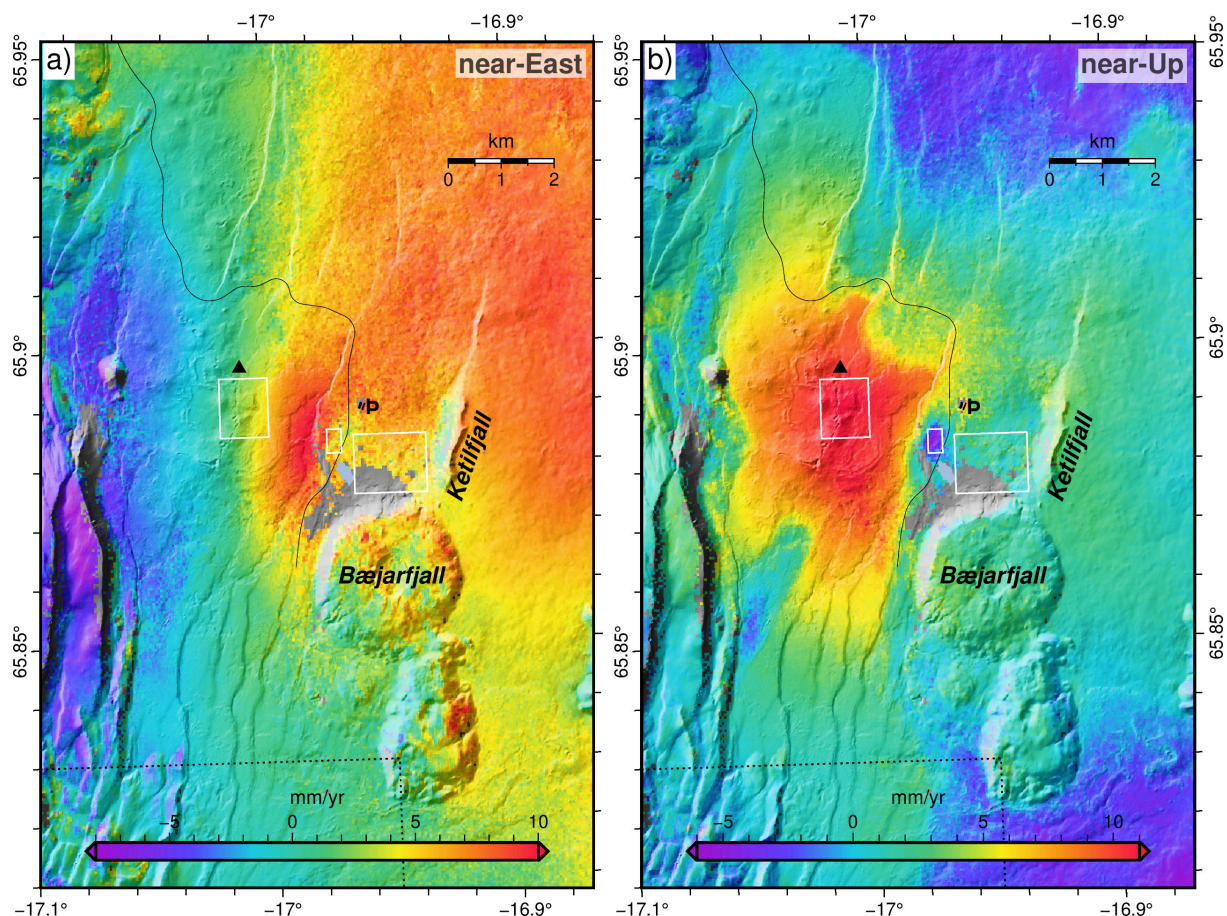


Figure 7: **(a)** Near-East and **(b)** near-Up velocities [mm/yr] between summer 2022 and summer 2023. Peistareykir power station (P) is indicated. The white boxes show the sampling area for the time-series plots. Velocities are referenced to the area delimited by the dotted line. Background shows shaded topography, the THRC continuous GNSS site (black triangle), and roads (thin lines).

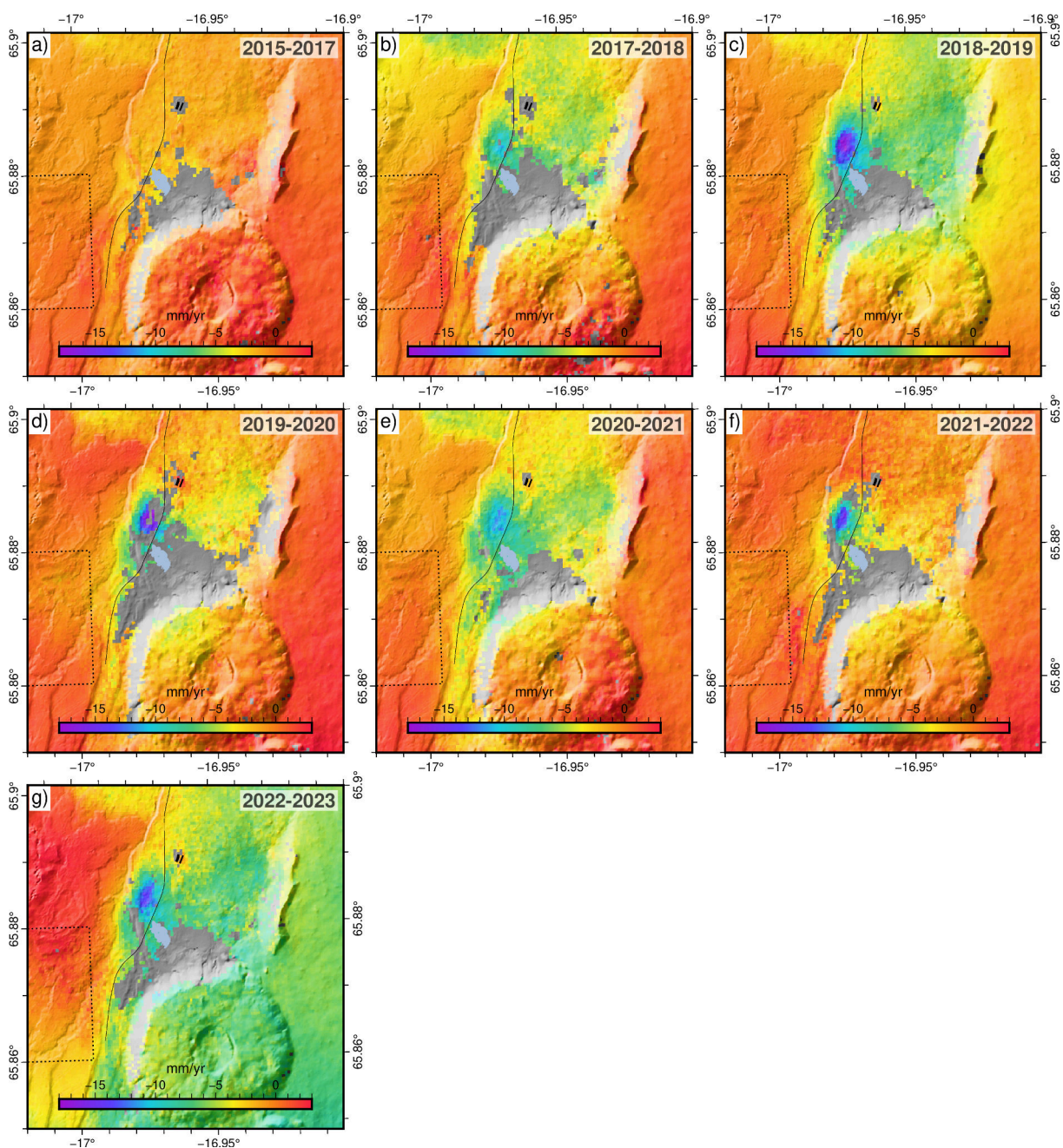


Figure 8: **(a)** Near-Up velocities [mm/yr] prior to production and **(b-g)** summer-to-summer velocities during production. Velocities are referenced to the area delimited by the dotted line. Background shows shaded topography and roads (thin lines).

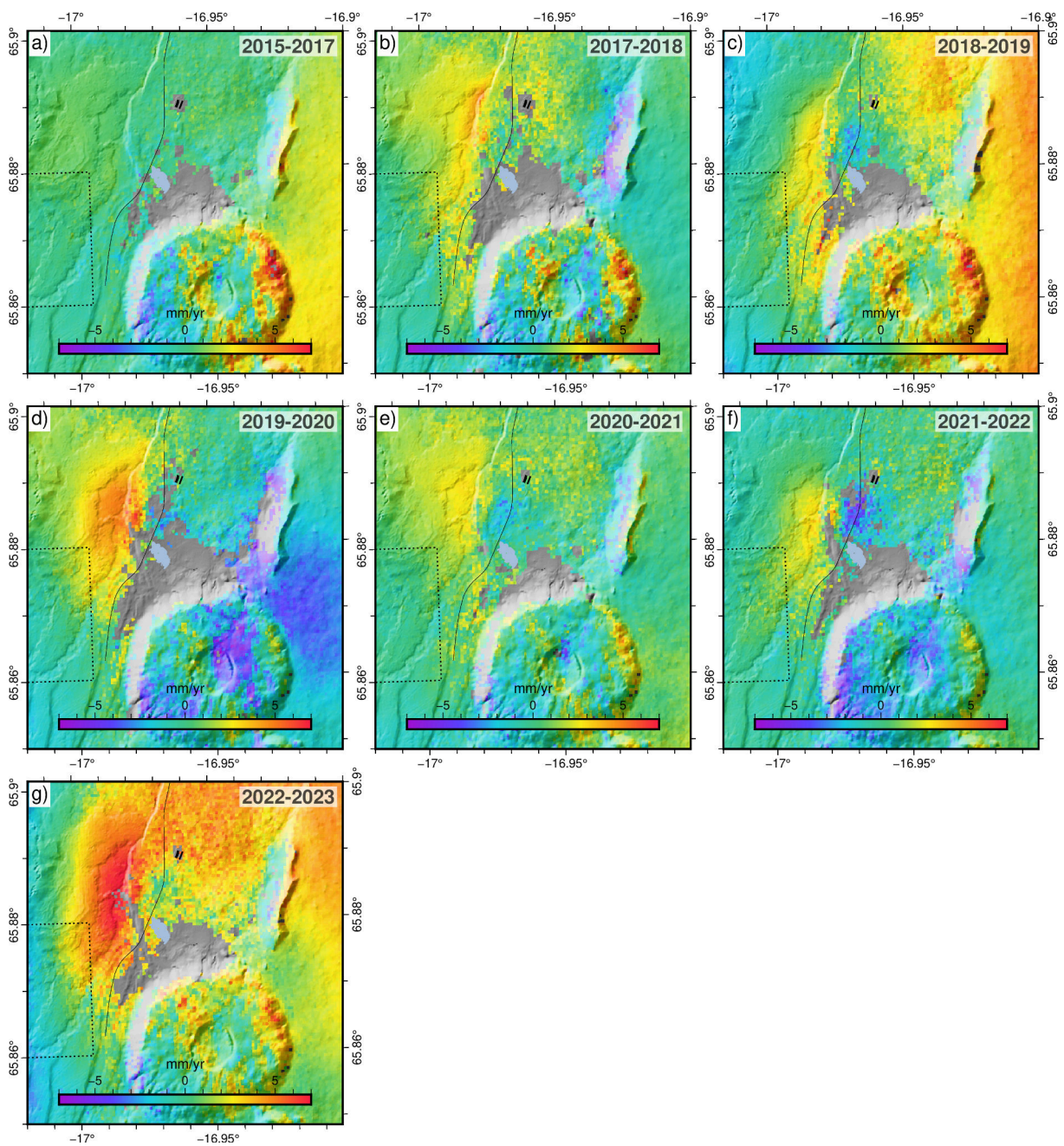


Figure 9: **(a)** Near-East velocities [mm/yr] prior to production and **(b-g)** summer-to-summer velocities during production. Velocities are referenced to the area delimited by the dotted line. Background shows shaded topography and roads (thin lines).

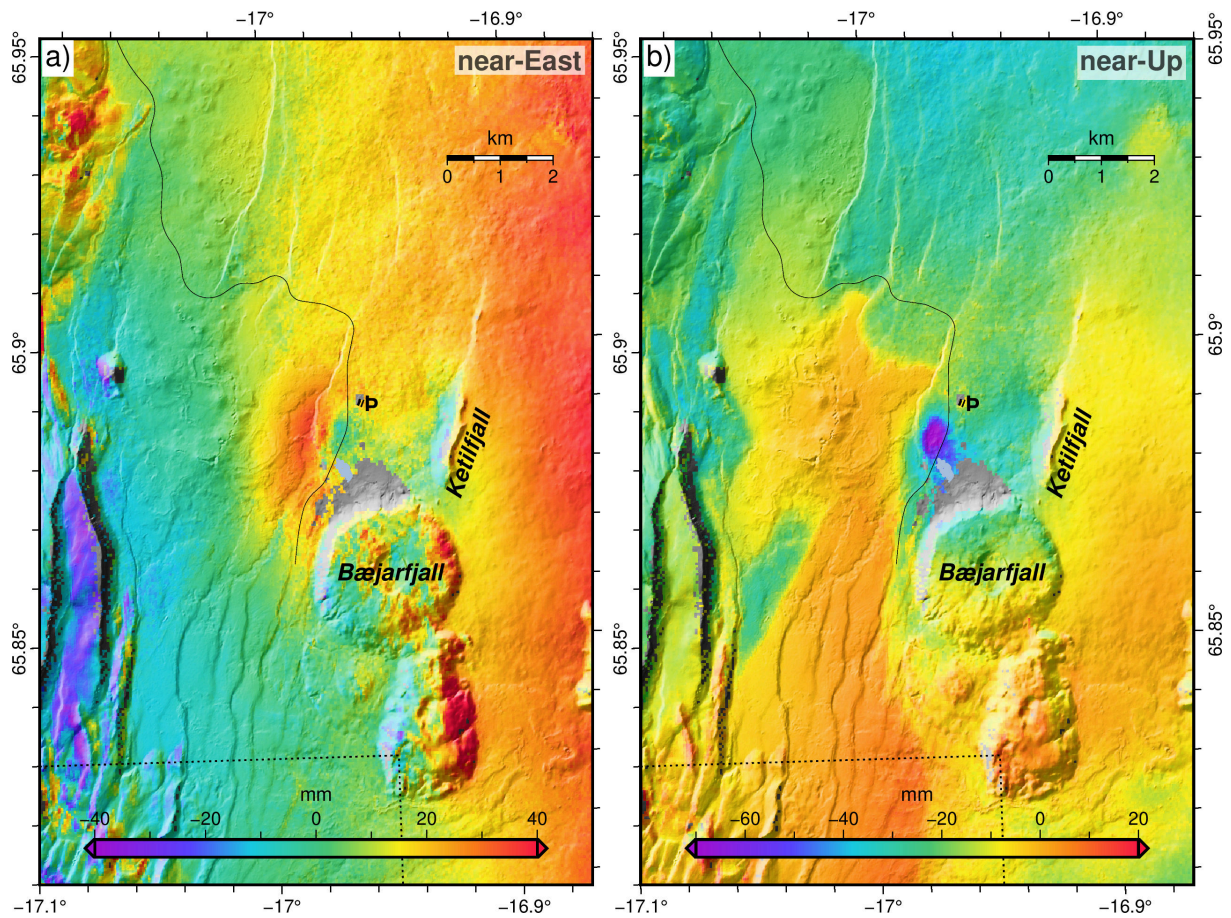


Figure 10: **(a)** Near-East and **(b)** near-Up total displacements [mm] between early July 2017 and end of September 2023. Peistareykir power station (P) is indicated. Displacements are referenced to the area delimited by the dotted line. Background shows shaded topography and roads (thin lines).

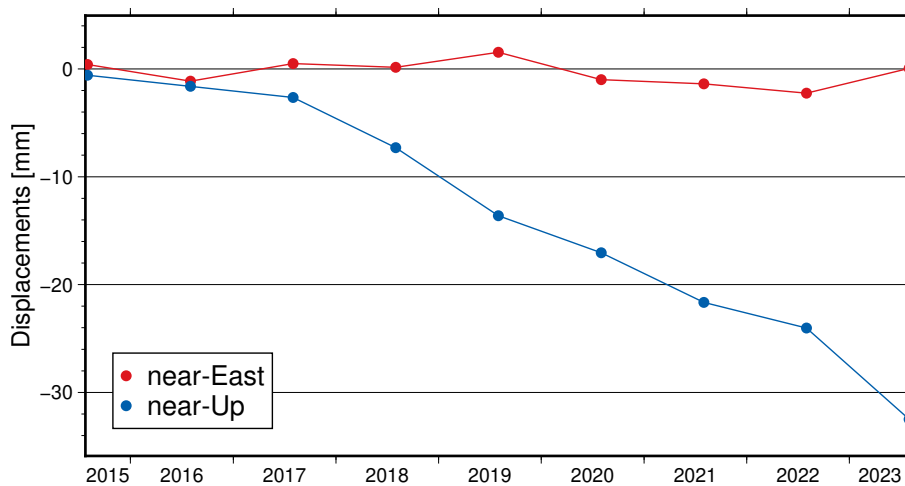


Figure 11: Near-East and Near-Up time-series of deformation north of Bæjarfjall since beginning of production in 2017. Location is indicated by the larger white box north of Bæjarfjall on Figure 7. Displacements are referenced to the area delimited by the dotted line on Figure 8.

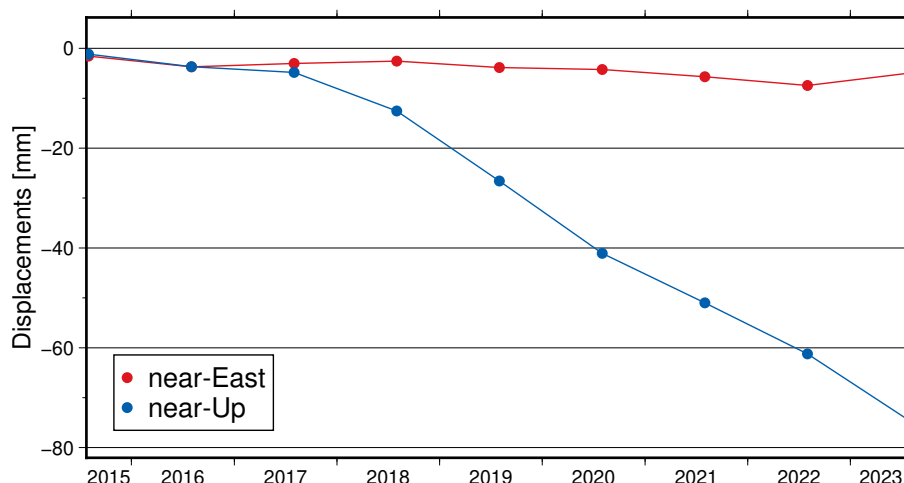


Figure 12: Near-East and Near-Up time-series of deformation at the maximum of subsidence since beginning of production in 2017. Location is indicated by the smallest white box on Figure 7. Displacements are referenced to the area delimited by the dotted line on Figure 8.

3.4 Peistareykir central volcano

A broad uplift is visible in the 2022-2023 velocities (Fig. 7). This uplift becomes very clear when looking at the deviation of the 2022-2023 velocities with respect to the 2017-2022 velocities (Fig. 13). The uplift is $\sim 12\text{-}15$ mm/yr between summer 2022 and summer 2023 (Fig. 14). Based on the visual inspection of the near-Up velocities, the center of the uplift is at about -17.01° longitude, 65.89° latitude (ISN93: 590700, 600700) (see location on Fig. 15). This is a very similar location to the one found for the center of the source behind previous inflation events (Metzger and Jónsson, 2014). The continuous GNSS site THRC, operated by the University of Iceland, is close to the center of the uplift and shows that uplift started around the beginning of 2023 (appendix Fig. 18). Therefore, the actual uplift rate is $\sim 20\text{-}25$ mm/yr.

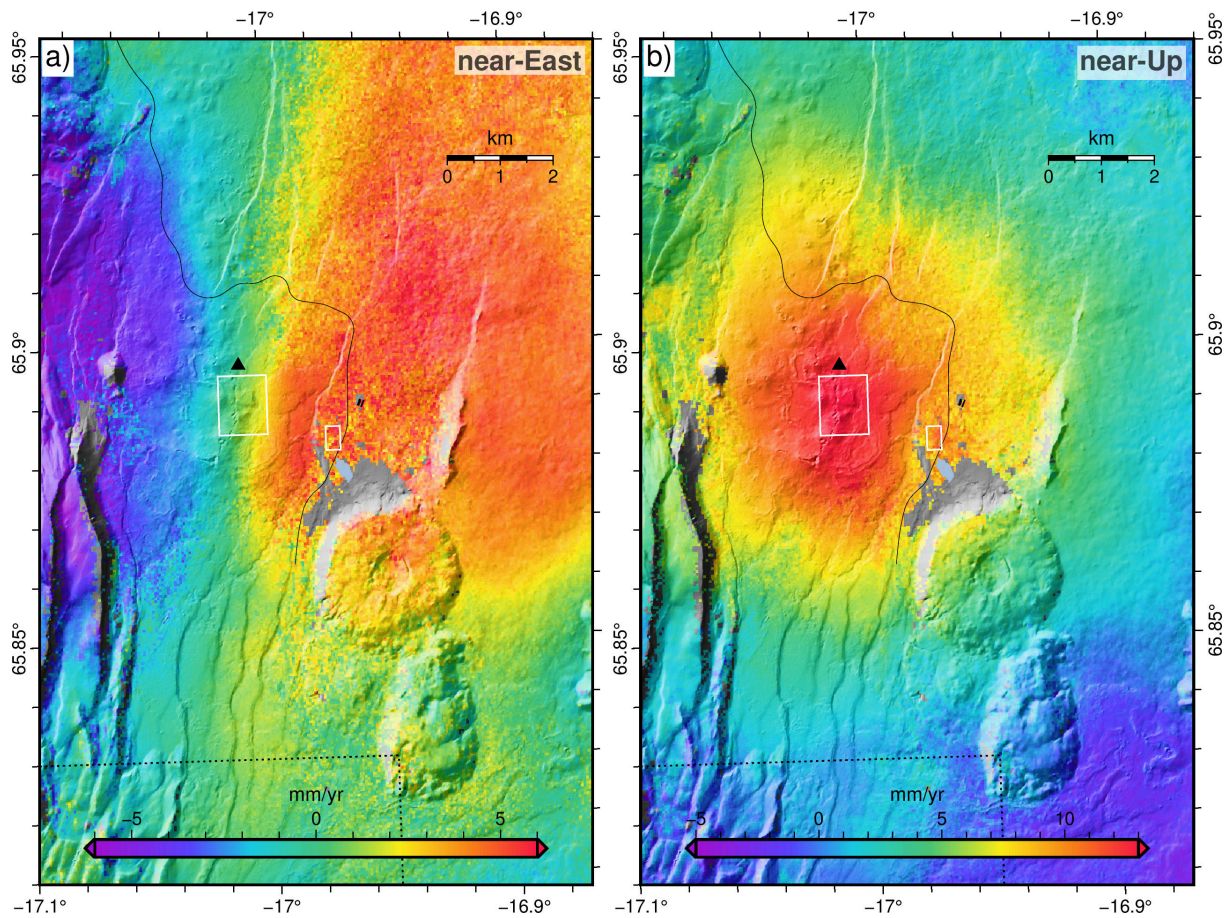


Figure 13: **(a)** Near-East and **(b)** near-Up velocities [mm/yr] of the difference between the 2017-2022 and 2022-2023 time spans. Velocities are referenced to the area delimited by the dotted line. The white boxes show the sampling area for the time-series plots. Background shows shaded topography, the THRC continuous GNSS site (black triangle), and roads (thin lines).

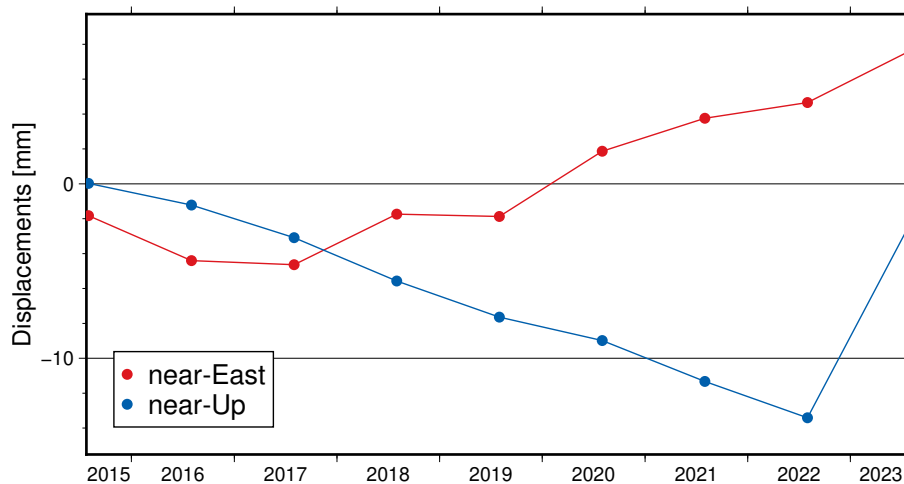


Figure 14: Near-East and Near-Up time-series of deformation at the maximum of the 2022-2023 uplift. Location is indicated by the white box on Figure 13.

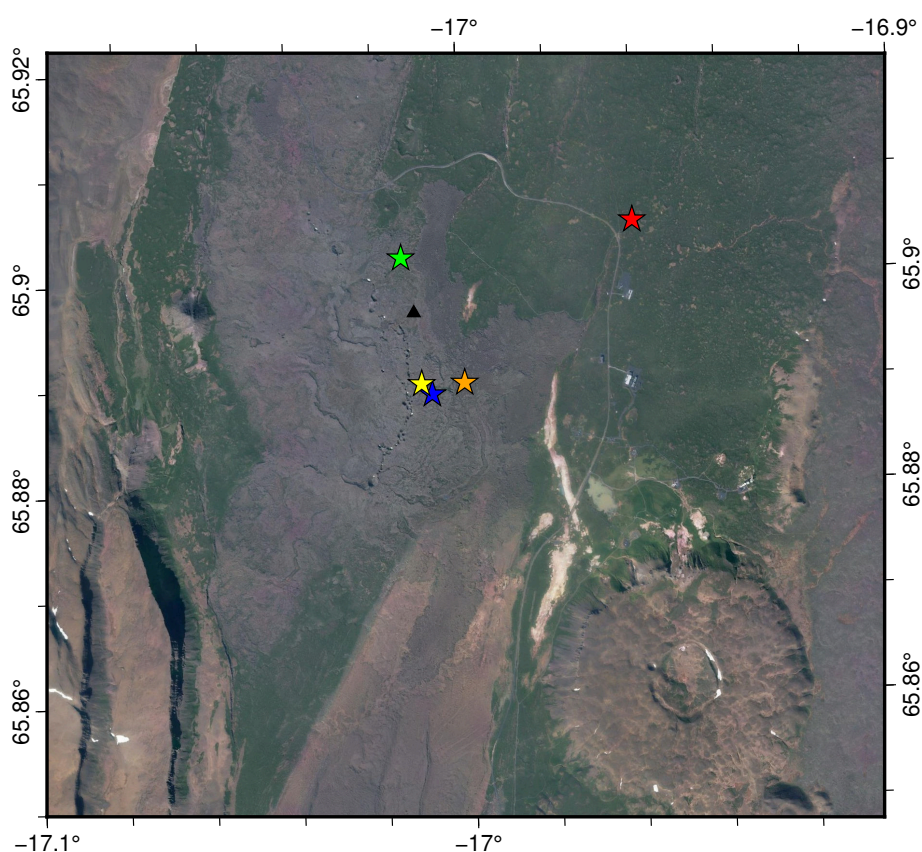


Figure 15: Map showing the center of the 2022-2023 uplift (yellow star), the center of the best-fitting Mogi model for the 2022-2023 uplift (green star), the center of the best-fitting Mogi model for the 2006-2009 uplift from Metzger and Jónsson, 2014 (blue star), the center of the best-fitting Mogi model for the 1995-1996 uplift (red star) and the 2006-2009 uplift (orange star) from Drouin, Sigmundsson, and Hreinsdottir, 2017, and the THRC continuous GNSS site (black triangle). Background shows aerial photography taken by Loftmyndir ehf in 2020.

Inversion modeling is used to estimate the location and volume of the source of this uplift. In regard to the circular uplift pattern measured at the surface, two models are considered for their simplicity and robustness: the Mogi model (Mogi, 1958) and the Okada dislocation model (Okada, 1992). The Mogi model is representing the inflow within a spherical magma body. The Okada model is representing a magmatic intrusion in the shape of a sill (an horizontal layer of magma within the host rock). In this inversion, the Okada dislocation is an horizontal square only allowing for tensile opening. The input to the inversion modelling are the three LOS 2022-2023 deviation from 2017-2022 velocity fields. They are down-sampled to keep the inversion time realistic. A simulated annealing approach with bootstrapping is used to estimate the best fitting model parameters and their 95% uncertainty. The inversion finds the best fitting model by minimizing the chi-square (χ^2) distribution. Two sets of models are run, defined on whether the horizontal position of the center of the model source was determined based on the center of uplift ("visual") or inverted for ("inversion"). Results are presented in Table 2. Visually, all models provide a good fit to the data ; no clear deformation pattern are left in the residuals (appendix Fig. 16-19). Mathematically, the Okada models provide a

slightly better fit to the data than the Mogi models. This can however be expected as the Okada model has three parameters (depth, width, opening) while the Mogi model has only two (depth, volume change). Mathematically, the "inversion" models also provide a slightly better fit to the data than the "visual" models. The "inversion" models are also deeper. This indicates that they are providing the best fit for a broader signal than the "visual" models which provide the best fit for the maximum of deformation.

Table 2: Modeling results

	Visual	Inversion
X (ISN93)	590700	590470 ⁺³³⁰ ₋₃₇₀
Y (ISN93)	600700	601950 ⁺⁴³⁰ ₋₃₄₀
Mogi (χ^2)	987	842
Depth [km]	4.4 ^{+0.9} _{-0.5}	5.0 ^{+0.8} _{-0.8}
Volume change [$\times 10^6$ m ³]	1.2 ^{+0.4} _{-0.3}	1.5 ^{+0.3} _{-0.4}
Okada sill (χ^2)	881	754
Depth [km]	7.2 ^{+6.5} _{-2.5}	8.1 ^{+5.3} _{-3.6}
Width [km]	1.4 ^{+2.9} _{-0.7}	1.6 ^{+2.9} _{-0.8}
Opening [m]	0.63 ^{+1.25} _{-0.5}	0.75 ^{+1.16} _{-0.54}
\leftrightarrow Volume change [$\times 10^6$ m ³]	1.2	1.9

4 Discussion

At Krafla, the deformation pattern shows a small uplift (~ 5 mm) on the west part of the caldera but nothing near the power plant between summer 2022 and summer 2023. However, when compared to the 2015-2018 deformation, we can instead see a ~ 7 -9 mm caldera uplift pattern centered around Leirhnjúkur (Fig. 2). This uplift is faster than during 2020-2022 but slower than the initial 2018-2020 uplift. It is not possible to determine what source is behind this uplift using deformation measurements alone. Combining this deformation dataset with seismic measurements, gravimetry measurements, and extraction/injection data might help to narrow the list of potential explanations for these variations of the local deformation.

At Hvíthólar, subsidence is observed. In the previous years, subsidence appeared to correlate with geothermal fluid extraction at the local borehole KJ-21 (Drouin, 2022).

At Bjarnarflag, the deformation pattern is the same since at least 1993 (Drouin, Sigmundsson, et al., 2017). There is a ~ 6 mm/yr subsidence bowl centered a few hundred meters west of the power plant. Geothermal fluids extraction from local boreholes has been relatively stable since deformation measurements have been conducted in the area. Therefore, assuming the observed deformation is related to this extraction rate, this would explain why the deformation rate is stable through time.

At the Þeistareykir geothermal field and its vicinity, the deformation pattern is the same since the start of production in 2017. There is a < 5 mm/yr subsidence area between Bæjarfjall and the power plant. This subsidence is likely related to the geothermal fluid extraction from

all the boreholes. However, the subsidence is the fastest (10-15 mm/yr) near the injection boreholes. There, the accumulated subsidence is more than 70 mm since 2017. This subsiding area is about 800 m long and 400 m wide, elongated along the fissure swarm direction. This suggests that the source of this deformation is shallow (< 1 km deep). The injection boreholes are about 400 m deep. Therefore it is likely that this local subsidence is related to the re-injection of geothermal fluids. However, the mechanisms behind this process are unclear as uplift, not subsidence, is usually expected from re-injection (Juncu et al., 2020). Potential explanations include i) fast cooling and contraction of the host rock by the cold re-injected fluids ii) chemical dissolution of a geological layer sensitive to water.

At the Peistareykir central volcano, a broad uplift is observed between summer 2022 and summer 2023. Two previous uplift episodes (1995-1996 and 2006-2009) have been observed since the beginning of geodetic measurement in the area (Metzger and Jónsson, 2014). The 1995-1996 deformation was 18 mm LOS and the 2006-2009 deformation was 78 mm LOS. For 2022-2023 the uplift was about ~ 12 -15 mm over ~ 7 month. The uplift rate is therefore fairly similar for all three inflation events at ~ 18 -26 mm/yr. For 2006-2009, Metzger et al. fit the deformation with a Mogi source with a volume increase of $25 \times 10^6 \text{ m}^3$ at 8.5 km depth. For 2022-2023, the deformation shows a good fit with a Mogi source with a volume increase $1.5_{-0.4}^{+0.3} \times 10^6 \text{ m}^3$ at $5.0_{-0.8}^{+0.8}$ km depth. It shows an equally good fit with a sill-shaped Okada dislocation with a volume increase of $1.9 \times 10^6 \text{ m}^3$ at $8.1_{-3.6}^{+5.3}$ km depth. The difference in depth for the 2006-2009 and 2022-2023 Mogi models indicates that the current source of uplift is shallower than before. However, it is important to remember that results are influenced by the inversion procedure adopted and input data. It is therefore recommended to validate these results by inverting both events using InSAR and GNSS data. Using GNSS data in the inversion would also help with constraining the shape of the source (Mogi-type or sill-type). The discrepancy in the location of the center of the "visual" models and "inversion" models could potentially be caused by broad atmospheric noise in the InSAR data. It could also indicate a more complex source geometry than the ones tested in this report.

References

- Berardino, P., Fornaro, G., Lanari, R., & Sansosti, E. (2002). A new algorithm for surface deformation monitoring based on small baseline differential SAR interferograms. *IEEE Transactions on Geoscience and Remote Sensing*, 40(11), 2375–2383. <https://doi.org/10.1109/TGRS.2002.803792>
- Drouin, V. (2020). *InSAR Monitoring of Krafla, Bjarnarflag and Peistareykir Geothermal Areas*. (tech. rep. No. ÍSOR-2020/43).
- Drouin, V. (2022). *InSAR Monitoring of Krafla, Bjarnarflag and Peistareykir Geothermal Areas, 2022 update*. (tech. rep. No. 22-001).
- Drouin, V., & Sigmundsson, F. (2019). Countrywide Observations of Plate Spreading and Glacial Isostatic Adjustment in Iceland Inferred by Sentinel-1 Radar Interferometry, 2015–2018. *Geophysical Research Letters*, 46(14), 8046–8055. <https://doi.org/10.1029/2019GL082629>
- Drouin, V., Sigmundsson, b., Verhagen, S., Ófeigsson, B. G., Spaans, K., & Hreinsdóttir, S. (2017). Deformation at Krafla and Bjarnarflag geothermal areas, Northern Volcanic Zone of Iceland, 1993-2015 [Volcano Geodesy: Recent developments and future challenges]. *Journal of Volcanology and Geothermal Research*, 344, 92–105. <https://doi.org/10.1016/j.jvolgeores.2017.06.013>
- Drouin, V., Sigmundsson, z., & Hreinsdóttir, S. (2017). Inflation events and quiescent periods since 1993 at Theistareykir central volcano, Iceland: role of magma intrusions for geothermal utilization [Portland, USA, 14-18 Aug. 2017]. *IAVCEI Scientific Assembly*, (PE41B-6).
- Einarsson, P. (1991). Umbrotin við Kröflu 1975-89. In A. Garðarsson & A. Einarsson (Eds.), *Náttúra Mývatns* (pp. 96–139). Hið íslenska náttúrufræðifélag.
- Juncu, D., Árnadóttir, T., Geirsson, H., Guðmundsson, G., Lund, B., Gunnarsson, G., Hooper, A., Hreinsdóttir, S., & Michalczewska, K. (2020). Injection-induced surface deformation and seismicity at the Hellisheidi geothermal field, Iceland. *Journal of Volcanology and Geothermal Research*, 391, 106337. <https://doi.org/10.1016/j.jvolgeores.2018.03.019>
- Metzger, S., & Jónsson, S. (2014). Plate boundary deformation in North Iceland during 1992–2009 revealed by InSAR time-series analysis and GPS. *Tectonophysics*, 634, 127–138.
- Mogi, K. (1958). Relations between the Eruptions of Various Volcanoes and the Deformations of the Ground Surfaces around them. *Bulletin of the Earthquake Research Institute*, 36, 99–134.
- Okada, Y. (1992). Internal deformation due to shear and tensile faults in a half-space. *Bulletin of the Seismological Society of America*, 82(2), 1018–1040. <http://www.bssaonline.org/content/82/2/1018.abstract>
- Rosen, P. A., Gurrola, E., Sacco, G. F., & Zebker, H. (2012). The InSAR scientific computing environment. *Synthetic Aperture Radar, 2012. EUSAR. 9th European Conference on*, 730–733.
- Sturkell, E., Sigmundsson, F., Geirsson, H., Ólafsson, H., & Theodórsson, T. (2008). Multiple volcano deformation sources in a post-rifting period: 1989–2005 behaviour of Krafla, Iceland constrained by levelling, tilt and GPS observations. *Journal of Volcanology and*

Geothermal Research, 177(2), 405–417. <https://doi.org/10.1016/j.jvolgeores.2008.06.013>

A Appendix

A.1 Krafla & Bjarnarflag

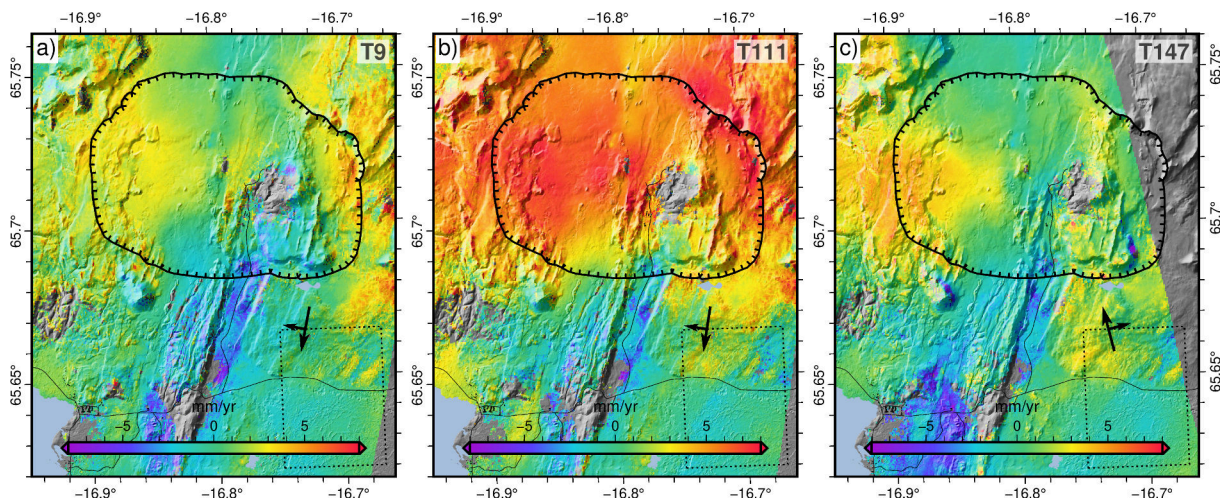


Figure 16: Average LOS velocities between summer 2022 and summer 2023 for all three Sentinel-1 track covering the area. Satellite heading and look direction is indicated by the large arrow and the small arrow, respectively. Background show shaded topography, the Krafla caldera boundary (comb line), roads (thin lines), and lakes (blue areas).

A.2 Peistareykir

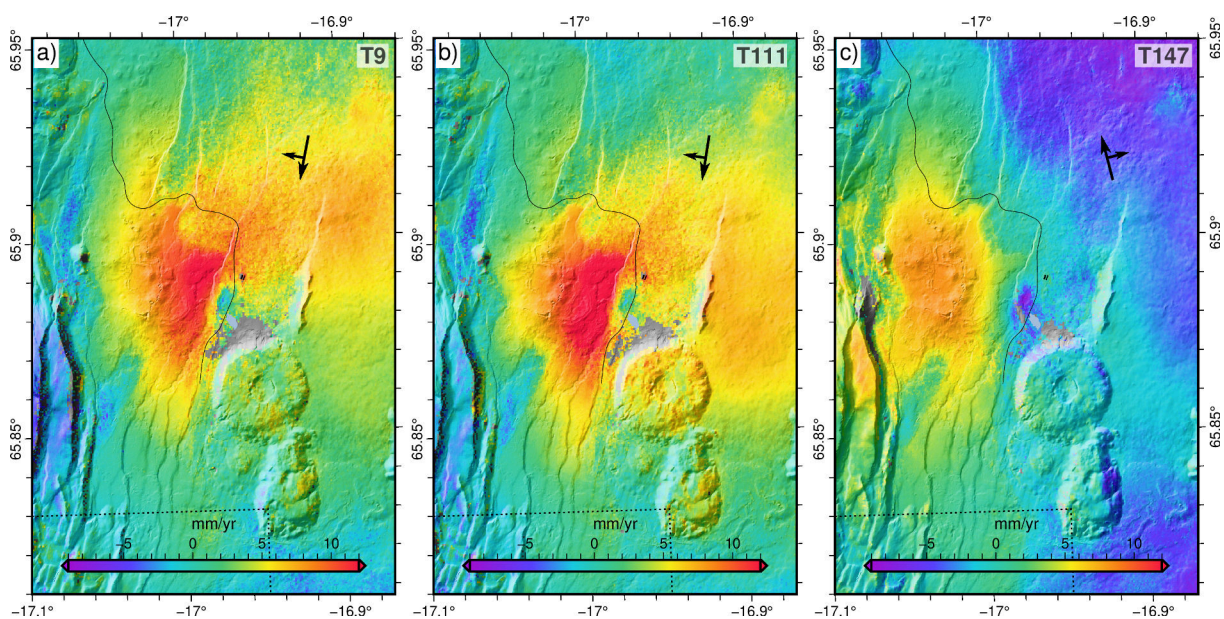


Figure 17: Average LOS velocities between summer 2022 and summer 2023 for all three Sentinel-1 track covering the area. Satellite heading and look direction is indicated by the large arrow and the small arrow, respectively. Background show shaded topography and roads (thin lines).

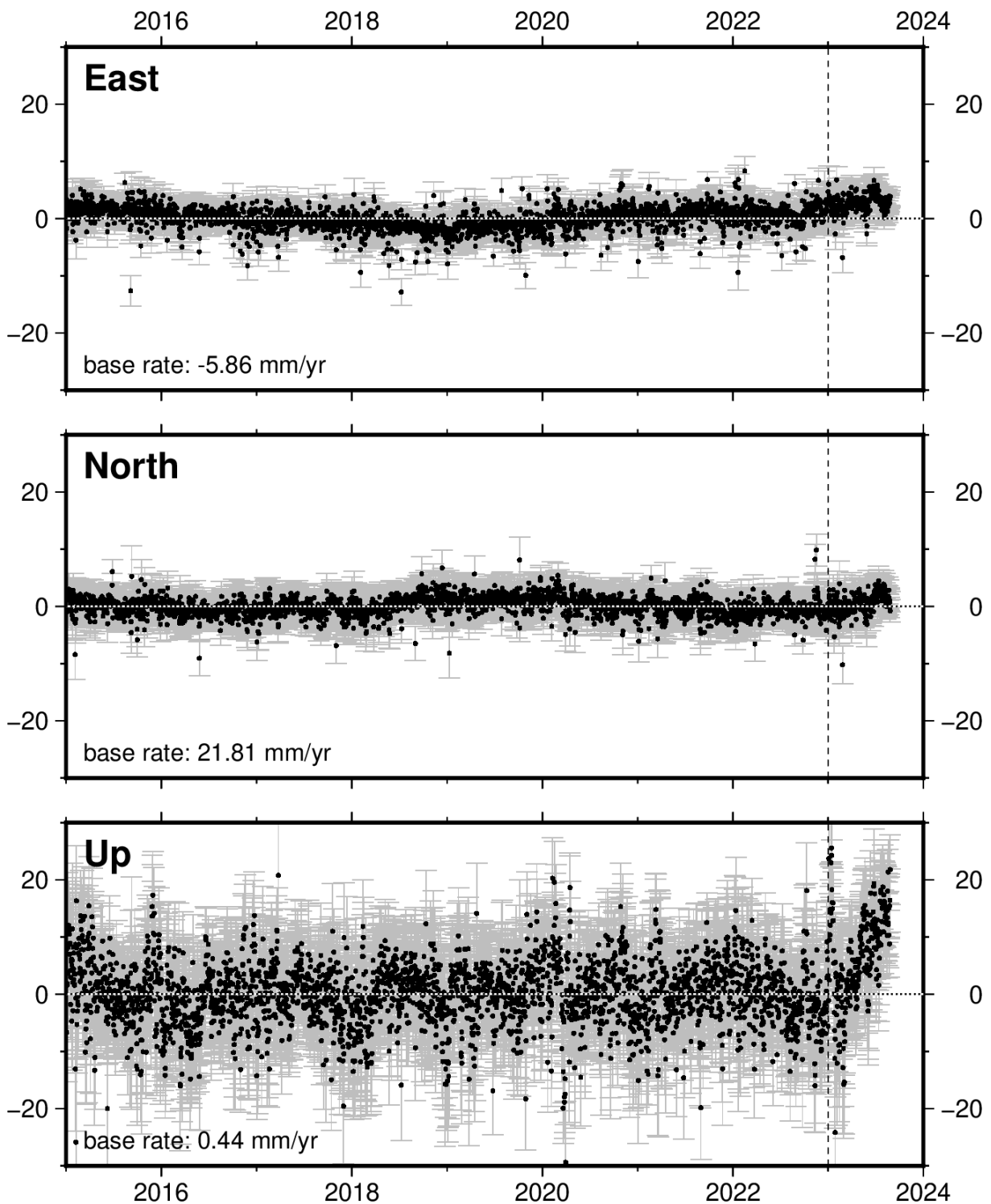


Figure 18: Time-series of the THRC continuous GNSS station. The time-series are detrended from the base rate until the end of 2022 (vertical dotted line) and the annual cycle to emphasize the deviation starting in 2023.

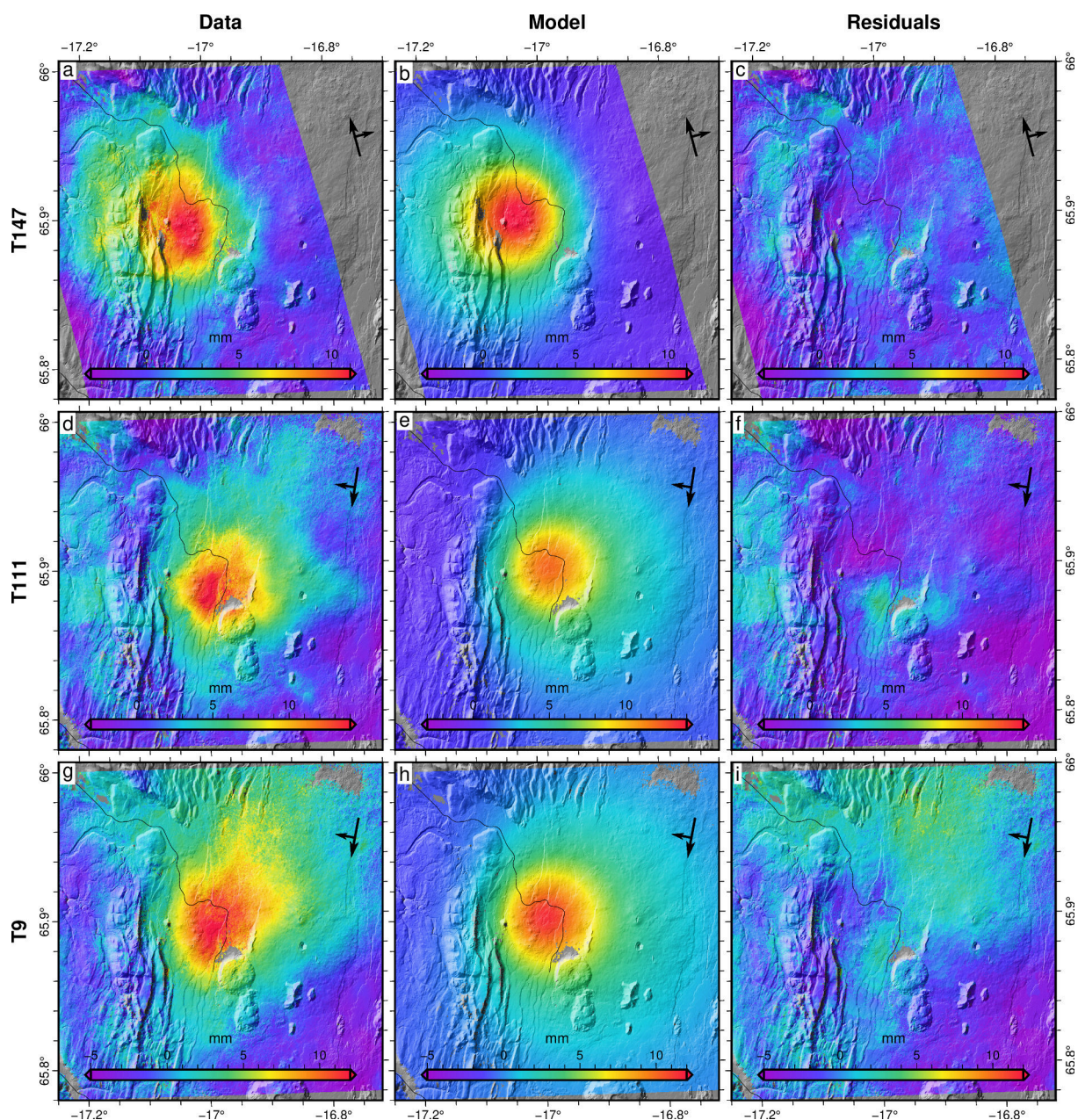


Figure 19: Data, best "inversion" Mogi model, and residuals for the three average LOS velocities between summer 2022 and summer 2023. Satellite heading and look direction is indicated by the large arrow and the small arrow, respectively. Background show shaded topography and roads (thin lines).

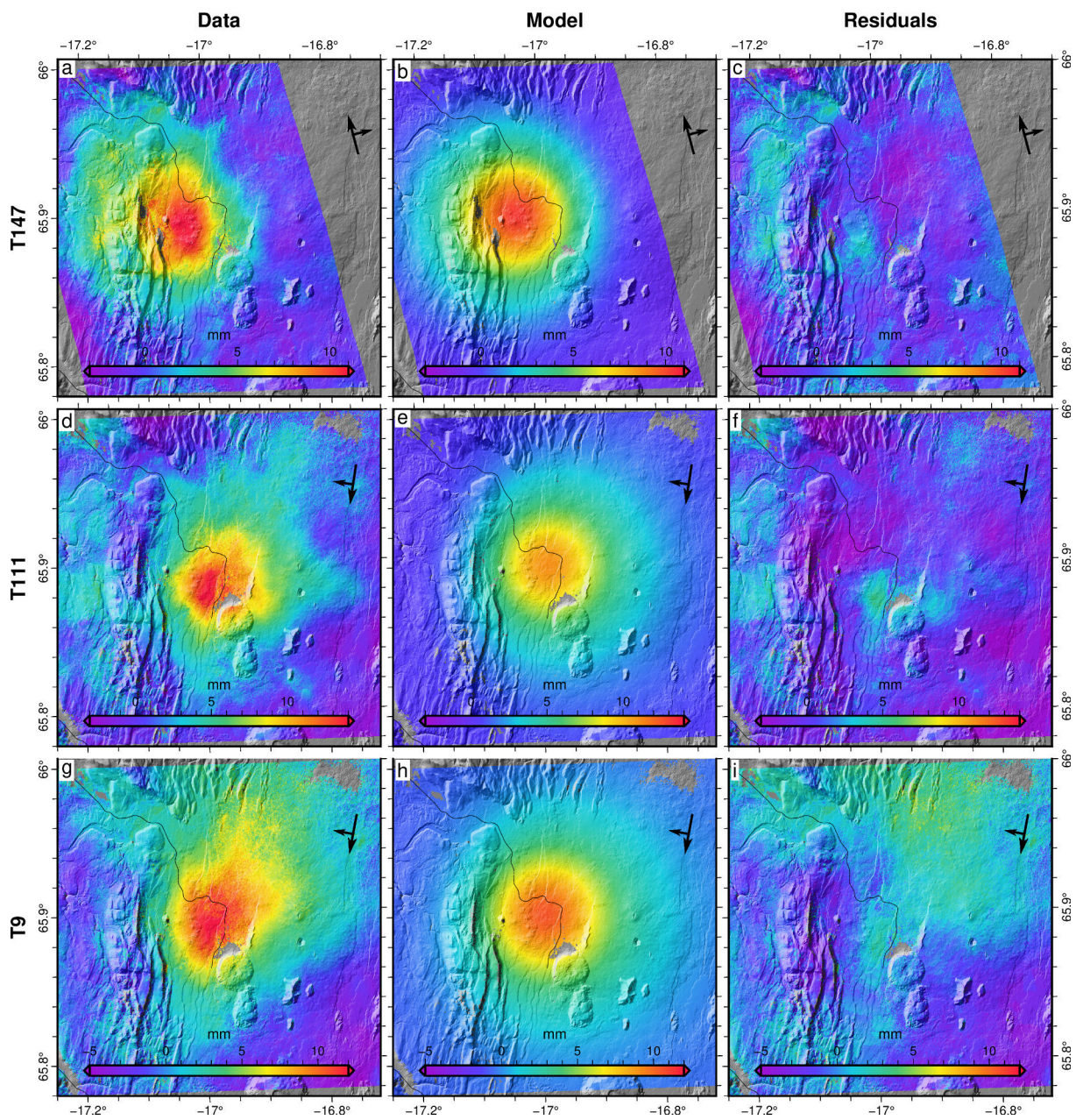


Figure 20: Data, best "inversion" Okada model, and residuals for the three average LOS velocities between summer 2022 and summer 2023. Satellite heading and look direction is indicated by the large arrow and the small arrow, respectively. Background show shaded topography and roads (thin lines).

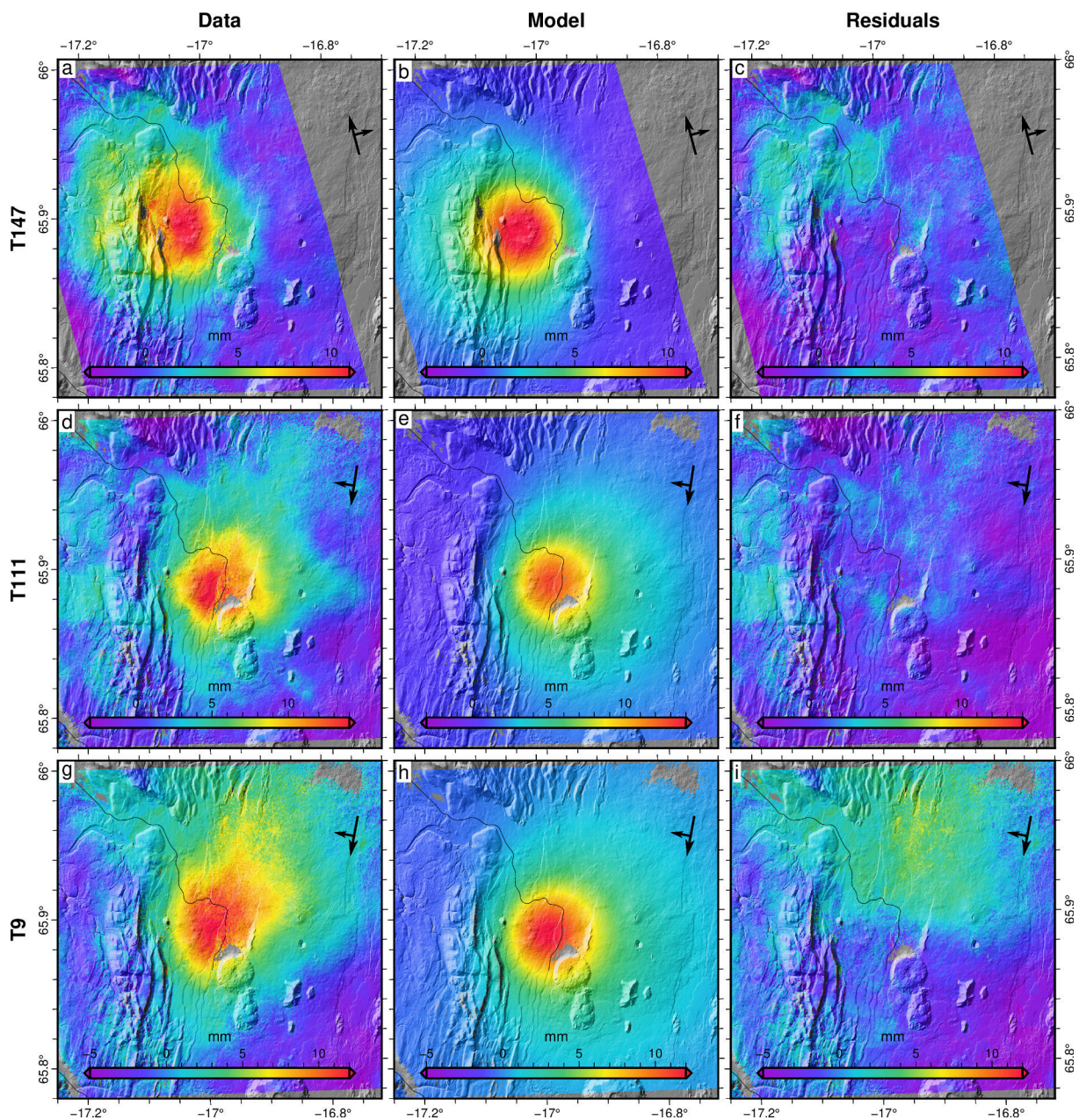


Figure 21: Data, best "visual" Mogi model, and residuals for the three average LOS velocities between summer 2022 and summer 2023. Satellite heading and look direction is indicated by the large arrow and the small arrow, respectively. Background show shaded topography and roads (thin lines).

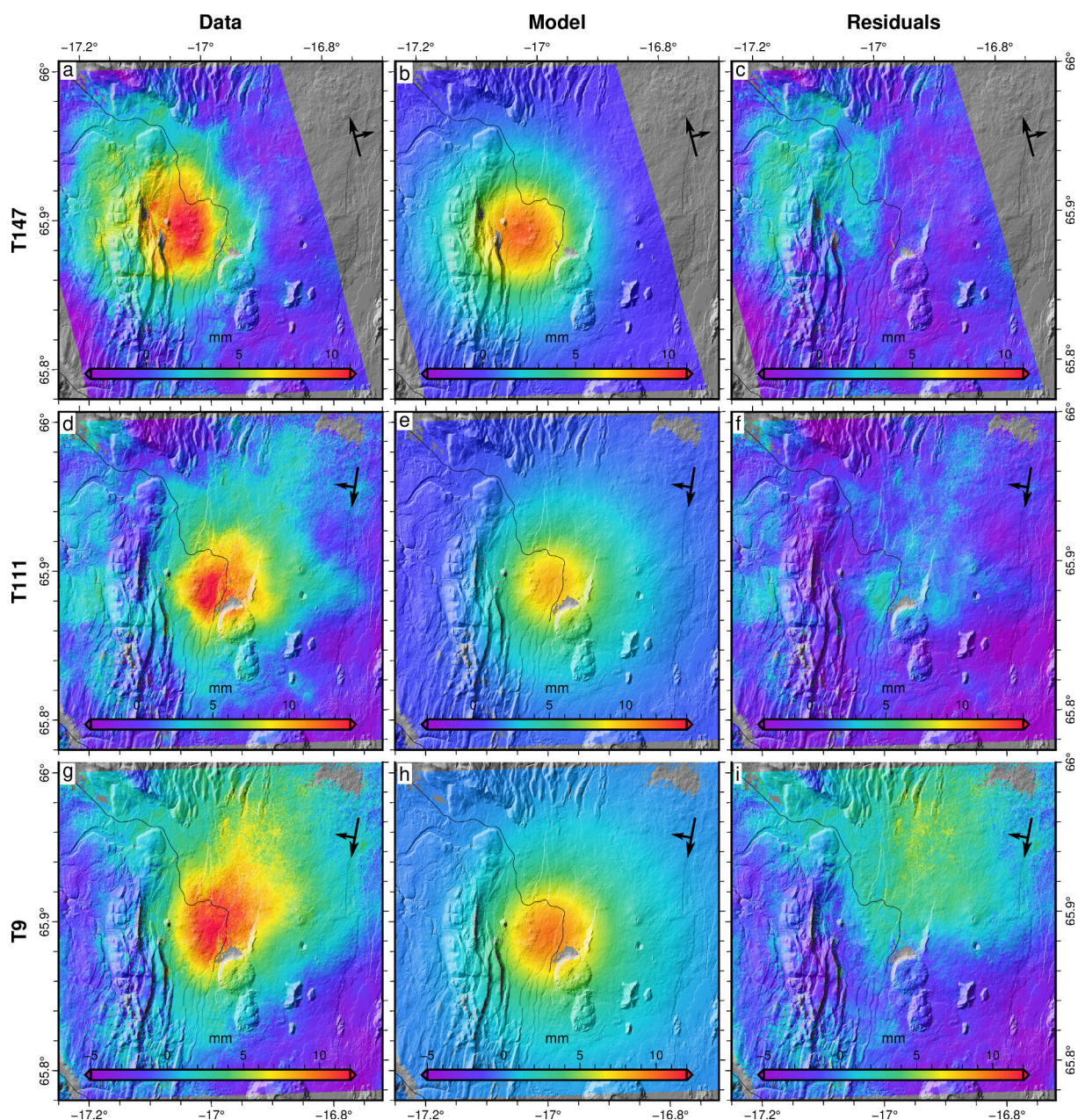


Figure 22: Data, best "visual" Okada model, and residuals for the three average LOS velocities between summer 2022 and summer 2023. Satellite heading and look direction is indicated by the large arrow and the small arrow, respectively. Background show shaded topography and roads (thin lines).